14

AFM and Cell Staining to Assess the *In Vitro* Biocompatibility of Opaque Surfaces

Christopher L. Frewin, Alexandra Oliveros,
Edwin Weeber and Stephen E. Saddow
University of South Florida
USA

1. Introduction

Although many current biomedical devices have been able to assist millions of people, there are still many critical needs to be addressed. Many individuals need constant diagnostics, controlled and targeted delivery of drugs, or even the replacement of motor and sensory functions. Many of the current biomedical systems that perform these functions are large, non-transportable, cumbersome or, more importantly, they cannot be in contact with the body for extended amounts of time. One solution is to utilize micro-electromechanical machines, or MEMS. With the same processes used to create computer chips, we can now generate a variety of micron sized machines which are designed to deliver drugs, detect physiological changes, and even electrically interface with cells. These micron to nanometer sized devices can potentially be implanted into the body with minimal invasiveness. There is, however, a very important issue which in turn needs to be addressed before their widespread clinical use can come to realization.

A major difficulty of long-term implantable MEMS devices is the body's inflammatory response to foreign materials. This has been termed the property of biocompatibility which is summarized as a material's ability not to illicit a negative physiological response while maintaining the devices designed functionality within the body environment (D. F. Williams, 2008). Materials need to be screened and verified for their biocompatibility before use within the human body. One problem is that many of the materials implemented in MEMS devices are opaque, which are difficult to examine for biocompatibility using traditional methods. For example, total internal reflection fluorescence (TIRF) measures the cell/ surface interface within 200 nm; however this technique nominally requires evanescent and internal reflection wave generation (Easley IV et al., 2008). Confocal microscopy generates point illumination of a sample through a combination of filters, beam splitters, and gratings to eliminate out-of-focus light, thereby detecting light within a specific focal plane, and raster scanning can then be used to generate detailed two and three dimensional images (Booth et al., 2008). Confocal microscopes are very expensive, and many of the models used typically in biology labs are designed with inverted microscopes not suitable for opaque substrates. Many fluorescent light microscopes suffer from the same limitations.

Atomic force microscopy (AFM) uses a laser reflected off a cantilever to gather quantitative morphological surface information, can image cells an opaque surfaces, and nominally costs

much less than a confocal microscope. It can provide information on cell spread and morphology on almost any surface. With this ability, the AFM can be used to investigate cellular activity on opaque materials. This chapter is dedicated to showing some of the methodologies we have developed to investigate biocompatibility of novel carbon materials.

1.1 Cellular to surface interactions

Examining the biocompatibility of a material for use in a medical device begins through the use of quantitative and qualitative techniques. These techniques have been collected into the International Standards Organization's (ISO) 10993 standards (ISO-10993-1, 2009; ISO-10993-5, 2009; ISO-10993-6, 2007). For *in vitro* testing, one of the most important qualifications is the interaction of cells on the surface of the material. Fig. 1 shows the process of cell attachment, which are mediated by the interactions between cell-surface integrin receptors and extra cellular matrix (ECM) proteins adsorbed on the substrate, in which the wettability, roughness, and charge of the surface play important roles (Lee, M.H. et al., 2005; McClary et al., 2000; Underwood et al., 1993). A biocompatible substrate will allow cells to perform required chemical processes on the materials surface, such as specific signal transduction responses, that lead to cell attachment and proliferation (Juliano & Haskill, 1993; Miyamoto et al., 1995).

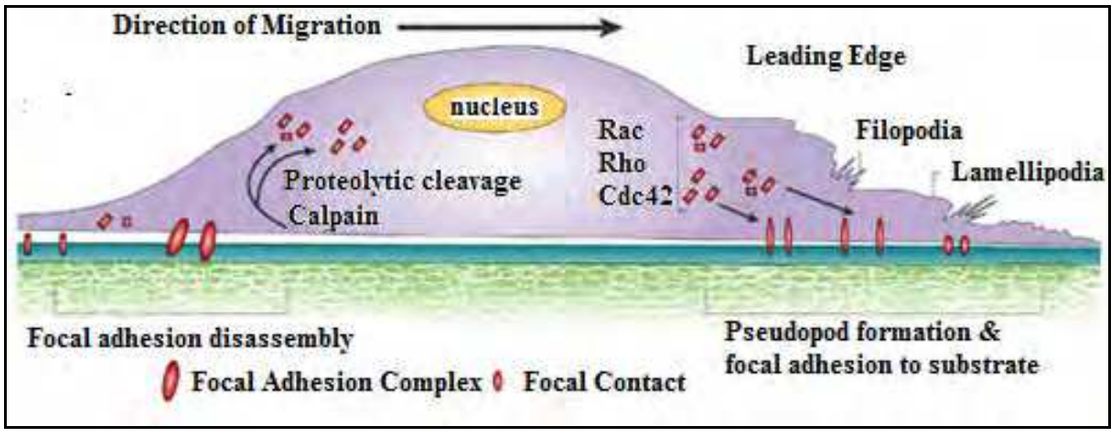

Fig. 1. A cartoon representation of cellular attachment factors to a substrate. The attachment involves focal adhesion complexes and contacts, filopodia, and lamellipodia (Frame et al., 2002).

Another measurement of surface biocompatibility is to evaluate the extension of lamellipodia or filopodia from motile cells onto a substrate surface (Levitan & Kaczmarek, 2002). Microtubule-filled growth cones, the backbone for dendritic spines and axons, are guided by the spike like filopodia and the membrane like lamellipodia (Levitan & Kaczmarek, 2002). The latter are attracted and repulsed by chemical and contact-mediated cues which influence how the structures connect to the outside world (Levitan & Kaczmarek, 2002). If an external surface is repulsive to the cells, these features will not couple with the surface and are retracted back into the central core, but if the substance is attractive, they couple strongly with the surface and new actin fibers flow to the leading edge (Levitan & Kaczmarek, 2002). Through the monitoring of lamellipodia or filopodia structures, a surface can be considered permissive to the cells if it produces attractive actions, and non-permissive if it repels them (Levitan & Kaczmarek, 2002).

1.2 Techniques used for study

For this chapter, we use three general methods to test our materials. Our first method was using MTT (3-(4,5-Dimethylthiazol-2-yl)-2,5-diphenyltetrazolium bromide) assay to quantitatively measure cellular viability/cytotoxicity on the materials. Our second method was AFM measurements to assess cellular morphology changes and lamellipodia/ filopodia permissiveness. Finally, we use immunohistochemistry to examine focal point adhesion and the actin mesh within cells on our substrates.

1.2.1 MTT assay

Cell viability/ cytotoxicity on the tested substrates were quantified using MTT assays. This proliferation assay was developed by Mossman and modified by Coletti et al. for bulk materials (Coletti et al., 2007; Mosmann, 1983). We take three 8 x 10 mm samples of the testing material, place them into a 12 or 24 well plate, and seed a predetermined number of cells (determined experimentally by previously producing 70 – 90% confluence layer) on each material and control. The cells are incubated at 37 °C, 5% CO_2, and 95% relative humidity for the time of the test without changing media. MTT, a chemical which is yellow in color, is added to each well (Mosmann, 1983). MTT is only metabolized by living mitochondria, with purple formazan as a by-product. We remove the remaining media carefully as to not disturb the formazan crystals, remove the samples from the wells, and place them into a 24 plate well (Coletti et al., 2007). This prevents corruption of the assay by adding formazan from cells attached to the polystyrene well to the formazan from material attached cells. Dimethyl sulfoxide, or DMSO, dissolves the purple formazan and is quantified by using a spectrophotometer measuring a wavelength of 500 to 600 nm (Mosmann, 1983). The MTT tests were repeated in triplicate for each tested material. The results from the MTT assays were normalized with respect to the control readings and expressed as the sampling distribution of the mean ($\bar{x}$) ± standard error of the mean (σ_M).

1.2.2 AFM techniques for live and fixed whole cells

This method was first reported in (Frewin et al., 2009b). AFM measurements are made using a Park Systems XE-100 AFM. Cells were seeded on each of the substrates within a 12 or 24 well plate incubated for at least 48 hours. The AFM of living cells was performed first within phosphate buffered solution, PBS, and provided the basis for a quantification of cell height, total surface area of the cell, angle of attachment, and the present extension of the lamellipodia/filopodia. The cells were then fixed using 4% paraformaldehyde for 20 minutes, which immobilized the lamellipodia and filopodia, and the cells were again measured using AFM. The measurements were repeated at least 3 times within each scan area, and are expressed as ratios or percentages to provide a basis for comparison. Analysis of the AFM images was performed with Park Systems XEI image analysis software as shown in Fig. 2(a).

Although the topographical measurement provided by AFM will not image the internal actin meshwork associated with lamellipodia and filopodia, these structures can still be identified and measured. It is the consensus view that filopodia are the cell vanguard for probing the local environment which is then followed by the generation of lamellipodia (Gordon-Weeks, 2004). By examining the sections of the outer extremities of the cell, we identified the spike-like

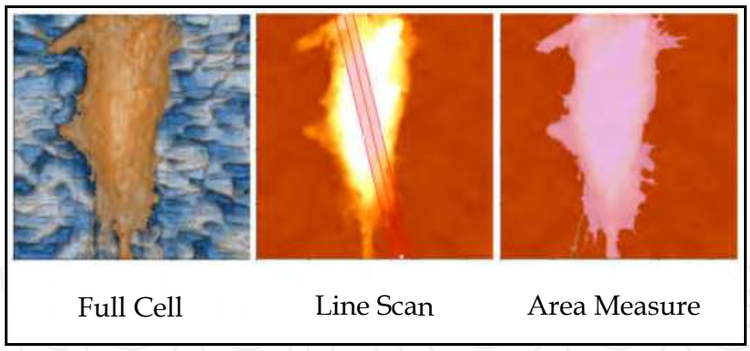

(a)

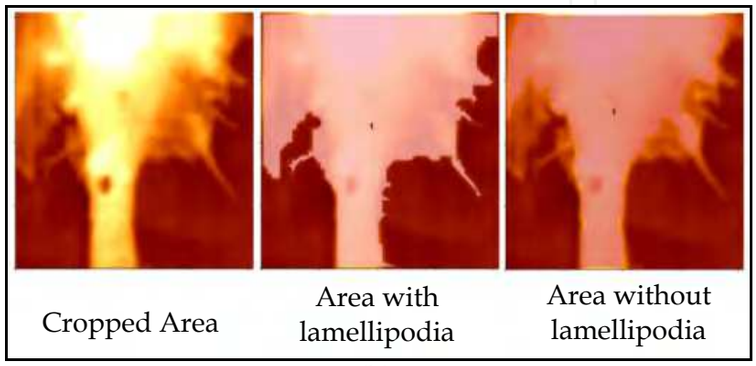

(b)

Fig. 2. Selection of 45 x 45 μm AFM micrographs utilized for cell permissiveness on the substrates. (a) From left to right: an enhanced color AFM micrograph of a cell, a line evaluation to determine cell height and angle of attachment, and a surface area measurement. (b) From left to right: a cropped 10 x 10 μm section of the AFM micrograph depicting filopodia/ lamellipodia, a full area measurement and an area measurement of the cell body eliminating the filopodia/ lamellipodia (Frewin et al., 2009b)

filopodia structures, as shown in Fig. 2(b). Lamellipodia are known to be a thin membrane layer 100 – 200 nm thick and parallel to the substrate surface (Gordon-Weeks, 2004). XEI area analysis was used on both living and fixed cell observations, normalized as a percentage of total cell attachment area, and the subsequent loss (or gain) percentage in area was used to quantitatively express the cell permissiveness to the substrate.

1.2.3 Immunohistological staining

To provide a clear picture of cellular attachment to a surface, we used immunofluorescence in one of our tests to examine the focal points and the actin cytoskeleton. We fixed the cells on our material using 4% paraformaldehyde, followed by a permeabilization and general antibody blocking for 2 hours with horse serum. The samples were then incubated with the primary antibody V4505 Monoclonal mouse anti-vinculin antibody (1:1000) in 4 °C overnight. The following day, we will conjugated the primary antibodies with goat anti mouse Alexa fluor 488 (1:250) for 2 hours at room temperature. We added rhodamine phalloidin (1:100) and ProLong® Gold antifade reagent with DAPI to stain the nucleus of the cells. The samples were viewed and recorded using a Leica DM2000 microscope with

EL6000 external light source. Microscope images were taken using a Canon Powershot S5 IS equipped with a Martin Microscope MM99 adapter.

2. Neuronal cellular interactions with opaque surfaces

The central nervous system, or CNS, is one of the most complicated systems in the body and consists of a dense network of neurons and glial cells. Implantation of a biomedical device into the CNS allows direct interaction with neural cells and effectively bypasses the blood-brain barrier. These devices can interact electrically with the CNS, be utilized as a platform for delivery of drugs, neural factors, proteins, genetic material, or even other cells to the CNS. These devices therefore can potentially repair a CNS system damaged by glial scarring due to trauma or disease (Stichel & Müller, 1998). Unfortunately, the construction materials for these devices activate microglia and astrocytes which begin to the process of gliosis, also referred to as the glial scaring (Fawcett & Asher, 1999).

The CNS response to chronic implantation is one of the greatest difficulties facing the widespread clinical incorporation of neutrally interfaced devices (Donoghue, 2008; Polikov et al., 2005). Not only is this reaction medically unsuitable, but neural implant (NI) devices which are electrode based are extremely vulnerable to changes in impedance and fail to function typically within months to a few years after glial encapsulation (Polikov et al., 2005; Rousche & Normann, 1998; J. C. Williams et al., 1999). Silicon (Si), a favored material for NI, is not chemically resistant and has been shown to consistently cause gliosis (Polikov et al., 2005; Rousche & Normann, 1998; J. C. Williams et al., 1999). Neural interfaces using SiO_2 and Si_3N_4 have shown gliosis also, but polyimide, a chemically resistive polymer material has shown excellent biocompatibility (Boppart et al., 1992; Rousche et al., 2001). Although this material offers excellent biocompatibility, displaying a fibroblast adherence, growth, and spread comparable to polystyrene, it has major drawbacks that hinder its acceptance as the material of choice for NI devices (Lee, K. K. et al., 2004). The material has a relatively high water uptake which decreases electrical impedance, and it is a very flexible material which add complications during NI implantation (Polikov et al., 2005).

A semiconductor material, silicon carbide (SiC), may offer a different approach to the generation of implantable neural MEMS devices. SiC has excellent mechanical properties, as it is incredibly hard but also possesses excellent elastic properties (Kordina & Saddow, 2004). SiC is chemically inert to acids, alkalis, and salts, does not absorb water and expand in liquid environments, and can be fashioned with many of the same processes used in the Si industry (Kordina & Saddow, 2004). More importantly, single crystal SiC is a semiconductor and therefore offers an alternative to Si as platform for the realization of NI devices.

Single crystal SiC has many different crystalline stacking sequences called polytypes, and each of these polytypes displays different electrical and mechanical properties. Although some literature exists on the biocompatibility of amorphous (a-SiC) and polycrystalline (poly-SiC), single crystal SiC needed more investigation (Kalnins et al., 2002; Li et al., 2005; Rosenbloom et al., 2004). This subsection reports on previously published research evaluating biocompatibility of cubic silicon carbide, 3C-SiC, nanocrystalline diamond (NCD), and silicon (Si) with immortalized neural cell lines (Frewin et al., 2009b). Cell treated polystyrene (PSt) and amorphous glass serve as negative and positive reaction control materials respectively.

2.1 Methods and materials

The samples used in this work were as follows: commercial (100) Si and (111) Si; (100) 3C-SiC and (111) 3C-SiC (growth process detailed in (Locke et al., 2009; Reyes et al., 2006)); NCD (process detailed in (Kumar et al., 2000)); amorphous glass cover slips; sterile Corning CellBIND® treated polystyrene. The Si and 3C-SiC were n-doped, possessing a negative bulk charge, and the NCD has intrinsic, or semi-insulating, doping. All samples were diced into dimensions of 8 mm x 10 mm. After dicing, the semiconductor and glass samples were ultrasonically cleaned in solvent baths of acetone, methanol, and isopropanol for 5 minutes each to remove dicing particulates and disinfect the surfaces. The semiconductor samples cleaned using the our standard cleaning process detailed in (Coletti et al., 2007; Frewin et al., 2009b). All H_2O was de-ionized (DI) with $\rho > 16$ MΩ cm. The PSt samples were cut with sterile scalpels within a class II A/B3 biological safety cabinet. All samples were placed into 70% (v/v) ethanol to prevent both bacterial growth and surface oxidation.

Two neural cell lines from American Type Culture Collection (ATCC) were used for this study; H4 human neuroglioma (#HTB-148), and PC12 Rat pheochromocytoma (#CRL-1721). The H4 cell line is derived from CNS glial cells and the PC12 is a neural modeling cell derived from the adrenal gland. The H4 cell line was cultured in advanced Dulbecco's Modified Eagle's Medium (DMEM) without L-glutamine supplemented with 10% fetal bovine serum (FBS), 2.2 mM L-glutamine, and 1% penicillin-streptomycin. The PC12 line was grown in Kaighn's F-12K Media supplemented with 2.5 % FBS, 15% horse serum, and 1% penicillin-streptomycin. The cells were cultured in Corning CellBIND® 75 mm^2 flasks to approximately 90% confluence, trypsinized, and enumerated using a hemocytometer.

Each sample was placed into a well of a 12-well plate. $1x10^5$ H4 cells and $5x10^5$ PC12 cells were seeded in each well followed with the addition of 3 ml of the appropriate media. After 96 hours, the MTT assay was performed in accordance with the procedures outlined in section 1.3.1. Amorphous glass was not tested in the MTT analysis due to numerous performance negative reports (Hench & Wilson, 1986). AFM procedures are detailed in 1.3.2.

2.2 Results

The MTT analysis results for both the H4 and PC12 cell lines are displayed in Fig. 3. The H4 cell line shows a viability level of approximately 80% ± 5% as compared to the PSt control for all samples excluding (111) Si, which performed at 108% ± 9%. The PC12 line indicates the 3C-SiC samples and (111) Si possess a proliferation greater than 90% of the PSt control, while the NCD and (100) Si possess proliferations of 46% and 55% percent, respectively. Fig. 4 displays selected AFM micrograph scans of the H4 and PC12 cell lines incubated on each of the tested substrates, and Table 1 summarizes the measurements of cellular morphology.

During the AFM measurement of both cell lines deposited on the various substrates, the Si surface was observed to suffer physical damage. Fig. 5 displays AFM scan micrographs of the semiconductor substrates before and after the cells had been deposited for a time of 48 hours. For each of the substrates seeded with cells, any cellular remnants and extracellular proteins were completely removed through the piranha cleaning method. Fig. 5a displays an AFM micrograph of the Si surface after the initial RCA cleaning, showing a surface marred by only a few nm deep polishing scratches, and it possesses a surface

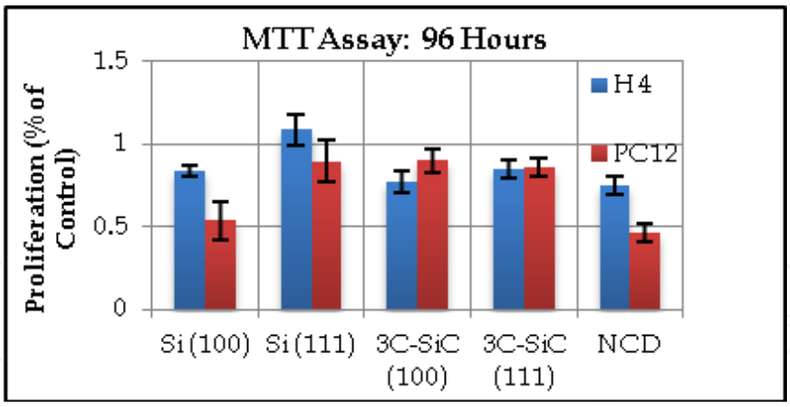

Fig. 3. The combined results of the MTT assay with the H4 and PC12 on our materials. The bars represent the SDM, $\bar{x}$, with error bars indicating the SEM, σ_M (Frewin et al., 2009b).

Cell Interaction with Substrate	Negative Interaction → → Positive Interaction				
H4 Cell Line	**Glass**	**PSt**	**Si**	**NCD**	**3C-SiC**
Live Cell Height/ Area (10^{-3} µm²)	7.04	5.40	3.11	3.82	4.58
Angle of Attachment (°)	23.80	30.60	15.20	13.80	16.30
% Area: Lamellipodia/Filopodia Reduction	27.00	13.50	10.00	8.10	-0.30*
PC12 Cell Line	**Glass**	**NCD**	**Si**	**3C-SiC**	**PSt**
Live Cell Height/ Area (10^{-3} µm²)	6.85	5.88	5.14	4.80	2.65
Angle of Attachment (°)	31.20	29.90	31.50	25.80	22.60
% Area: Lamellipodia/Filopodia Reduction	24.80	19.50	10.20	4.50	-3.30*

Table 1. Values for the cell-surface interaction measured with AFM (Frewin et al., 2009b).

root mean square (RMS) roughness, r_q in 5 x 5 µm of 0.137 nm. The surface of the Si after the cell deposition (not shown) indicates many large elliptical depressions approximately 100 – 200 µm long which roughly correlate to the shapes of the H4 or PC12 cells. The surface within the depressions, which is displayed in Fig. 5b, shows numerous small, rounded pits with diameters of 500 to 700 nm and ranging from 30 to 70 nm deep. These features increased 5 x 5 µm r_q to 18 nm RMS.

3C-SiC and NCD are known to be chemically inert materials and they therefore do not display the changes seen on the surface of the Si substrates. The surface of 3C-SiC, displayed in Fig. 5c & 5d show a rough, mosaic surface due to planar defects caused by the 20% lattice mismatch between 3C-SiC and Si, but no pitting or cellular damage. The deposited NCD shows the microcrystalline grain structures across the surface. The 3C-SiC has a 5 x 5 µm r_q of 2.46 nm RMS before and after cell seeding. NCD has much more surface variation as indicated by the differences in Fig. 5e and 5f, and shows 5 x 5 µm scan size r_q of 17.79 nm RMS and 13.42 nm RMS before and after cell seeding.

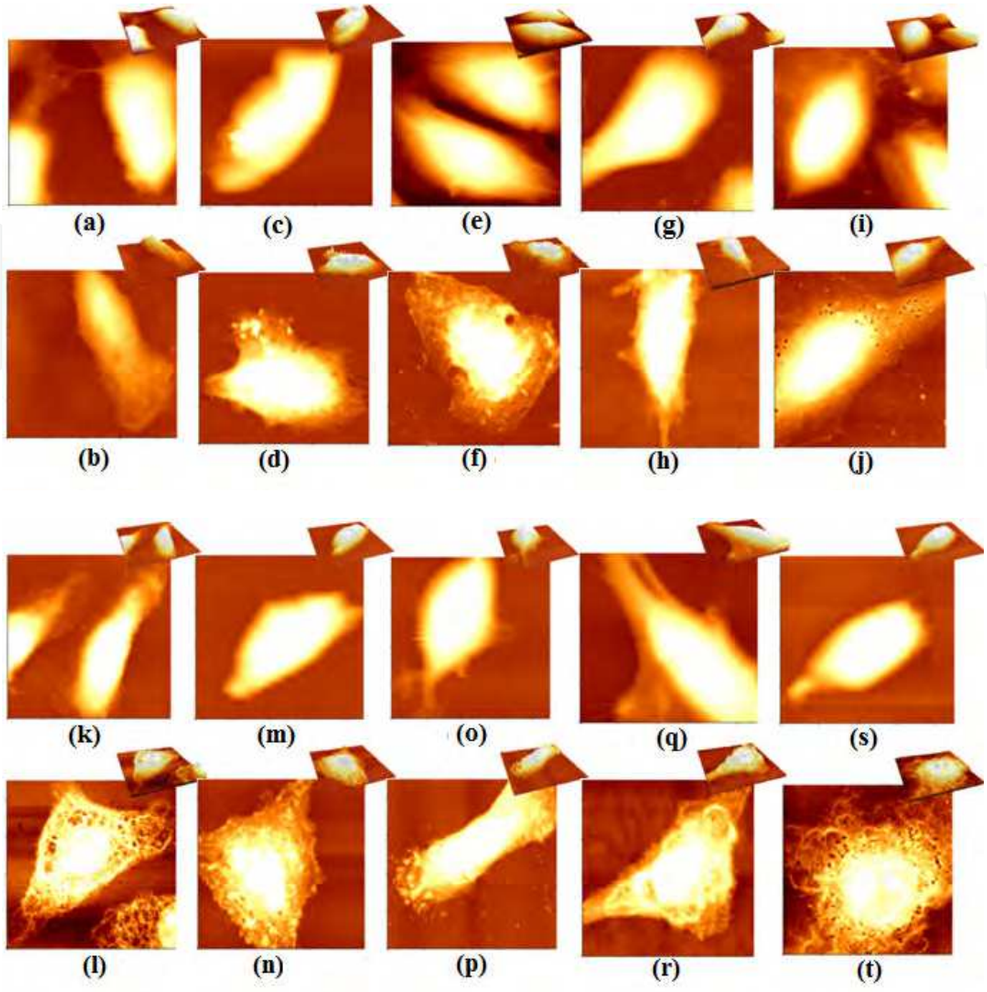

Fig. 4. 45 x 45 µm AFM micrograph of H4 andPC12 cells on the substrates. (a), (c), (e), (g), and (i) are live H4 cells measured in PBS deposited on PSt, glass, Si, 3C-SiC, and NCD respectively. (b), (d), (f), (h), and (j) are have been fixed on PSt, glass, Si, 3C-SiC, and NCD. (k), (m), (o), (q), and (s) are live PC12 cells measured in PBS deposited on PSt, glass, Si, 3C-SiC, and NCD respectively. (l), (n), (p), (r), and (t) are have been fixed on PSt, glass, Si, 3C-SiC, and NCD (Frewin et al., 2009b).

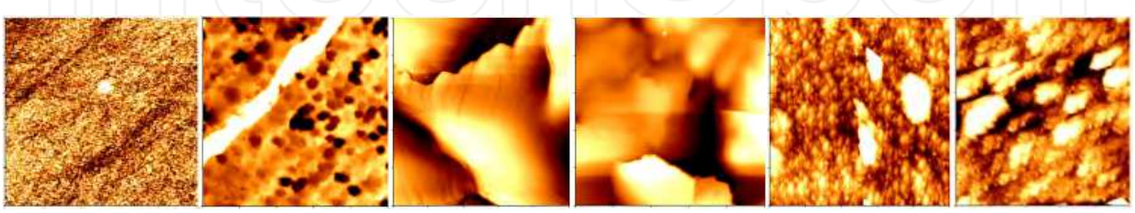

Fig. 5. 5 x 5 µm AFM micrographs of the surfaces of the three tested semiconductors. (a) and (b) are Si, (c) and (d) are 3C-SiC, and (e) and (f) are NCD before and after removal of cells. Note that Si shows signs of surface modification where NCD and 3C-SiC are relatively unchanged (Frewin et al., 2009b).

2.3 Discussion

This study focused on gaining insight of the biocompatibility of bare, untreated substrates with immortalized neuronal cell lines, and primarily used two factors to determine the level of biocompatibility. MTT assays, shown in Fig. 3, were used to determine cell proliferation and viability, and the AFM measurements, compiled in Table 1 and Fig. 4, were used to determine cell morphology for information on cell to substrate interaction and the permissiveness of the substrate. Cell proliferation and subsequent membrane attachment on substrates is dependent on a complex combination of physical, electrical, and chemical reactions which are influenced by both surface and bulk substrate properties and the cell membrane structure (Kumari et al., 2002; Richards, 1996). Cellular attachment to a substrate involves the absorption of proteins within the media serum to its surface, followed by cellular membrane integrin interactions (Rouhi, 1999). Subsequent membrane attachment, membrane spread, and cellular growth are controlled by internal cellular cues initiated by integrins, and it has been demonstrated that the response is heavily mediated by the surface wet-ability and surface charge (Kim et al., 2001; Rouhi, 1999). Hydrophilic and charged surfaces allow fibronectin (Fn), an extracellular protein which allows cell membrane to surface binding, to unravel and elongate as it is absorbed onto the surface, whereas hydrophobic surfaces show Fn is absorbed in its natural, compact, and rounded form (Bergkvist et al., 2003). Cells show little reactivity with Fn in solution, so elongation is one important factor for cell membrane reactions to occur (Bergkvist et al., 2003). Furthermore, cell charge and surface wet-ability have been indicated as very influential factors for both surface interaction and neurite growth and guidance. Growth cone formation and filopodia/ lamellipodia guidance have been shown to favor a more hydrophobic surface (Clark et al., 1993). Neurite formation and extension are also influenced by substrate charge, with this growth favoring positive charge over negative charge, and neutral charges produce almost no neurite outgrowth (Fine et al., 1991; Makohliso et al., 1993).

PSt treated through oxygenation for optimal cell attachment was used as a normalizing control for the MTT assay test and as a comparison for cell attachment in the AFM analysis. Proliferation of the H4 and PC12 was higher than the tested substrates with the exception of (111) Si for the PC12. The level of attachment of the cells to the PSt substrate showed some variation in that the AFM analysis indicated that the PC12 showed a low surface profile and large surface area spread for the cell membrane, while the H4 have a large angle of attachment, a subsequent high surface profile, and less surface area membrane attachment. The lamellipodia permissiveness was also much better for the PC12 than the H4 on this surface. This material has been shown to be normally hydrophilic, as indicated by (Kim et al., 2001), and the Corning data sheet provides a H_20 contact angle of 12.3° - 16.3°. This material has been also shown to often possess a negative surface charge (Bergkvist et al., 2003). The hydrophilic surface and the negative charge of this material would allow for elongation of the attached proteins, and therefore could be a reason the cells have high proliferation. The negative charge could also be a reason for the improved cell attachment and lamellipodia extensions for the PC12, as was also found with (Fine et al., 1991). However (Makohliso et al., 1993) showed evidence that CNS neurite growth was more sensitive to charge and favored a more positively charged environment, and this may be a reason for the decreased H4 and lamellipodia attachment.

The untreated amorphous glass substrate surface was evaluated in this study as it is more hydrophobic than 3C-SiC and slightly less hydrophobic than Si, PSt and NCD, respectively

as seen by (Sklodowaka et al., 1999) which reports a contact angle of 51.05°. Amorphous glass would also not provide a net substrate charge as it is an insulating material but any charges that contact the surface would remain in place. The AFM analysis shows that both cells tend to greatly minimize their contact with this substrate and have little lamellipodia surface attachment, although cells on this substrate displayed large areas of lamellipodia probing, which is consistent with past observations (Bergkvist et al., 2003). The neutral charged surface could be a large factor in inhibiting the neurite expansion, as was shown by previous studies (Fine et al., 1991; Makohliso et al., 1993).

Both faces of Si have shown a measured contact angle of 65.85° (Coletti et al., 2007), indicating a weakly hydrophobic surface. The samples were doped n-type providing a negative charge potential within the bulk of the material. The H4 showed good viability for both Si surfaces. The PC12 results indicated poor cell viability for (100) Si, but excellent cell viability for (111) Si, while the AFM indicates a high cell profile, large angle of attachment, and a moderate lamellipodia attachment. As Si is hydrophobic, and the samples possess negative potential, the differences between the reactions of the cells to the PSt may be due to their chemical properties. The evidence may be displayed in Fig. 5d which indicates some chemical reaction on the Si has occurred when cells are present. Also, studies have indicated the presence of Si compounds present in the CNS (Birchall & Chappell, 1988). Both cell lines have much higher proliferation on the (111) Si face than the (100) Si face, which may be due to the available dangling surface bonds. The lower viability of the PC12 on (100) Si is not so easily explained, but the lower attachment quality shown by the AFM analysis indicates Si is not entirely favorable for this cell. The reaction of the cell and the substrate may be forming silicic acid, which can have a negative effect on the cell viability when present in large quantities (Carlisle, 1986). The moderate lamellipodia attachment to Si is most likely due to the negative charge of the substrate, and mirrors the results seen by (Fine et al., 1991; Makohliso et al., 1993), but attachment of the lamellipodia may have been altered due to the hydrophobic substrate surface (Clark et al., 1993).

Both faces of 3C-SiC, unlike Si, have high proliferation values for both cell lines when compared with the PSt control, and the surface, shown in Fig. 5e, showed no adverse effects of surface degradation through cellular interaction on the surface. The AFM indicated that the H4 have good cellular spread, low profile, and excellent lamellipodia permissiveness. A low angle of attachment, moderate cell spread, and a relatively good level of lamellipodia attachment was also observed for the PC12. The same difference in viability that was observed in the Si crystalline planes also exists with 3C-SiC. (Coletti et al., 2007) have shown the USF 'as grown' 3C-SiC has a contact angle of 52.53°, and (Yakimova et al., 2007) indicates that SiC contains both hydrophilic and hydrophobic sites due to its alternating elemental surface. It should be noted that these substrates are negatively charged, although at a level much lower than the Si substrates. The fact that this substance is hydrophilic and has viability levels comparable to the hydrophobic Si, along with the observation that there is a similar viability contrast between the crystal orientations, suggests that there may be competing bonding principals. One hypothesis is Si is the prevalent membrane bonding site on 3C-SiC and Si substrates, but the patchy C surface bonds slightly decrease the attachment sites, and thus viability, on 3C-SiC. However, the bonds involved for these cells are relatively strong, as indicated by the flattened cell profiles. Like PSt and Si, the negative material charge and presence of hydrophobic sites on 3C-SiC would generate good lamellipodia extension, but the greater attachment of the lamellipodia may be due to the hydrophobic sites on the surface caused by the patchy C bonding sites.

Intrinsic NCD shows a good level of viability, cellular membrane expansion, and attachment with the H4. Alternatively, the high cell profile and poor viability shows the PC12 does not favor NCD. The H4 shows a moderate level of lamellipodia attachment, and the PC12 line shows a very poor level of lamellipodia attachment. NCD has been shown by (Ostrovskaya et al., 2007) (via contact angle measurements of 75° - 95°) to be a hydrophobic surface which is mainly due to the large amount of sp2 bonded graphitic defects along the crystal grain boundaries. As the NCD is intrinsic, there should be no appreciable surface charge level, but random charges may be present along defect boundaries, and the underlying n-type Si substrate may produce capacitive effects. The PC12 follows the previous studies of (Kim et al., 2001; Rouhi, 1999) which show a low cellular viability and attachment due to a hydrophilic surface. The low lamellipodia attachment may be due to the intrinsic charge as was seen in (Fine et al., 1991; Makohliso et al., 1993). The H4 cell line, however, does not follow previous observations. Further exploration into the surface properties of NCD and how this material interacts with extracellular proteins would be necessary to determine reasons for the observed level of viability.

2.4 Conclusion

This initial study of neural cell interaction with 3C-SiC and NCD has provided evidence that these materials may be suitable for use in a NI device, but further investigation is needed to examine the neuron cell reaction on these substrates. 3C-SiC indicated that both cell lines used in this study showed a relatively high level of cellular viability as compared to PSt that has been treated for optimal cell viability. Cell morphology results showed that the cells attach very well to 3C-SiC, and. it has excellent lamellipodia permissiveness which is an important quality for NI devices. Furthermore, the chemical resilience of 3C-SiC demonstrates that this material resists the surface degradation that was observed on the Si surfaces. The as-grown NCD showed good viability and moderate permissiveness for the H4 cell line, but has a poor performance with the PC12 line. Future experiments need to be conducted to better understand the cellular membrane molecular interaction with the surfaces of 3C-SiC, Si, and NCD as many questions regarding substrate charge and protein reactivity remain unresolved.

3. Cellular interactions with Self-Assembled Monolayer (SAM) surfaces

An ideal biosensor would consist of a biocompatible material that could be functionalized to achieve a specific aim, such as detection of target bio-molecules or promotion of specific protein attachment (Vahlberg et al., 2005). Self assembled monolayers (SAM) modified surfaces yield inorganic/organic interfaces which can be used to tailor the surface properties of SiC to achieve a specific aim. Previous studies of SAM formation on Si, glass, and gold surfaces have proven many of these surfaces are highly biocompatible, with corresponding increases in cell adhesion which facilitated the identification of protein adsorption (Kapur & Rudolph, 1998; Low et al., 2006; Mrksich & Whitesides, 1996). SAMs are composed of organic molecules that are covalently immobilized on the surface of the semiconductor via suitable linker groups (Catellani & Cicero, 2007; Stutzmann et al., 2006). In general, hydrogen (H) or hydroxide (OH) terminated surfaces provide the reactive sites necessary to obtain high quality monolayers. Hydrosilylation and silanization are two common surface functionalization processes used extensively on Si substrates (Linford & Chidsey, 1993; Stutzmann et al., 2006), and SAMs have been

analyzed in detail, with suppression or enhancement of cell spreading and proliferation depending on the SAM molecular end-group (Faucheux et al., 2004). In this section, we report on the results of our study on the biocompatibility of SAM surface-functionalized hexagonal silicon carbide, 6H-SiC, where the SAM surfaces produced both hydrophobic and hydrophilic surfaces. The biocompatibility was assessed through the AFM and MTT assay techniques detailed in 1.3.1 and 1.3.2.

3.1 Methods and materials

Two (0001) 6H-SiC 3.43° off-axis, n-type, 420 μm thick were diced into 5 x 5 mm die. First, we performed hydrogen etching in order to obtain well-ordered, atomically flat surfaces with reduced surface defect densities (Frewin et al., 2009a). The samples were cleaned as described in section 2.1. followed by a 5% diluted HF dip that results in OH termination of the surface (Li et al., 2005).

After cleaning and etching the samples, alkylation of (0001) 6H-SiC was performed by reaction of the hydroxylated surfaces with 1-octadecene for 120 min at 200°C under Ar. The samples were then ultrasonically cleaned in hexane, chloroform, and methanol for 10 min each (Schoell et al., 2008; Sharp et al., 2008). The silanization reactions were performed by immersing the samples in 10% APDEMS (or APTES) in anhydrous toluene for 90 min at room temperature in an N_2 environment, followed by ultrasonic cleaning in toluene and isopropanol for 20 min each (Schoell et al., 2008). After SAM formation, the samples were placed in 70% (v/v) ethanol to prevent bacterial growth.

Static water contact angle measurements were performed using a KSV CAM101 system from KSV Instruments. A 3 μl droplet of DI water was deposited on three different samples for each of the surfaces prepared. The droplet contact angle was determined by measuring the angles between the baseline of the drop and the tangent of the same. In addition, AFM topography measurements of the surfaces were performed.

We utilized the two ATCC neural cell lines, H4 and PC12, for this investigation. The same culture methods in 2.1, were used. The experimentally determined MTT assay cell seeding concentration was $5x10^5$ cells/ml for both the H4 and PC12 cell lines. The same amount of cells were seeded on samples and placed in 12 well plates for the evaluation.

3.2 Results

The results of this study have been previously reported in (Oliveros et al., 2009). Static water contact angle (SWCA) measurements give an idea of the degree of hydrophobicity and hydrophilicity of the functionalized substrates. Table 2 contains the SWCA and RMS roughness values for the surfaces tested. We observed a hydrophobic surface for the 1-octadecene-treated sample, consistent with methyl molecular end-groups (Schoell et al., 2008; Sharp et al., 2008). The APDEMS and APTES surfaces were moderately hydrophilic, similar to the expected values for amino end-groups (Schoell et al., 2008). The untreated sample exhibited hydrophilic behavior, consistent with a native oxide. Surface topography analysis with AFM showed a very smooth surface following etching and prior to functionalization (~ 0.3 nm RMS). The 1-octadecene-treated surface showed a similar topography to the pre-functionalized 6H-SiC surface, no aggregates (See Fig 6 b). On the

Substrate	Surface Roughness[1)] (r_q, nm RMS)	Contact angle (°)[2)]
6H-SiC H_2 etched	0.30	19 ± 2
6H-SiC with Octadecene	0.26	110 ± 5
6H-SiC with APDEMS	0.36	48 ± 4
6H-SiC with APTES	0.53	54 ± 2

[1)] RMS is the mean of 5 scans over a 5 µm x 5 µm.
[2)] Contact angle is the mean of 3 measurements for a 3 uL H_2O droplet on different surfaces.

Table 2. SAM characterization via AFM and water contact angle analysis (Oliveros et al., 2009).

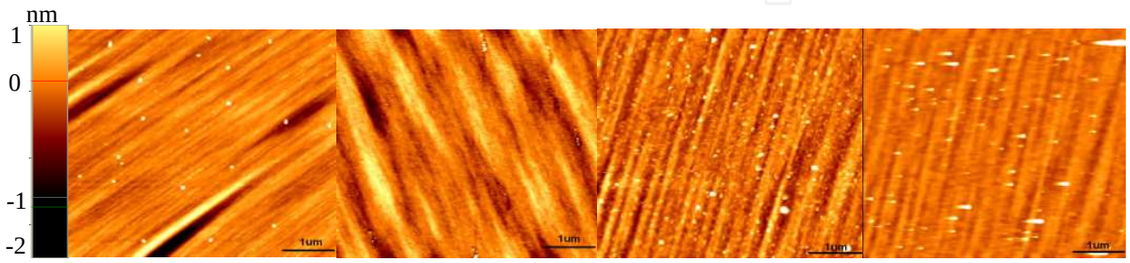

(a) (b) (c) (d)

Fig. 6. 5 µm x 5µm AFM micrographs of (a) 6H-SiC, (b) 6H-SiC after alkylation, (c) 6H-SiC APDEMS and (d) 6H-SiC APTES. AFM data taken in tapping mode (Oliveros et al., 2009).

other hand, the APDEMS and APTES functionalized surfaces show some signs of polymerization, most likely due to homogeneous methoxy cross-linking, which were observed as particulates and a difference of r_q with respect to the 6H-SiC substrate (see Fig. 6c & 6d).

MTT assays were performed and normalized to the PSt control to quantify the cell viability on (0001) 6H-SiC without surface treatment and functionalized with the three SAM compounds. Fig. 7 indicates both cell lines show similar viability trends; however, the PC12 show lower levels of relative proliferation. For the H4 seeded on unmodified 6H-SiC, we obtained proliferation of only 31 ± 1% relative to PSt. The cell viability increased for the 1-octadecene functionalized surface by 240 ± 3% relative to the untreated surface, whereas the APDEMS and the APTES treated surfaces showed dramatic increases in cell proliferation, exceeding the untreated surface value by 670 ± 4% and 850 ± 5%, respectively. The PC12 cells displayed a lower proliferation on 6H-SiC of only 38 ±3% relative to PSt. The 1-octadecene functionalized surface results with the H4 show a 171 ± 3% increase of proliferation relative to untreated 6H-SiC. The APDEMS functionalized surface yielded a 320 ± 4% proliferation to the 6H-SiC, whereas cell proliferation for APTES increased 480 ± 4%. More importantly, these results show a statistically significant degree of higher cell proliferation than previous studies done with PC12 cells on porous Si (Low et al., 2006) and SAMs on Si and glass substrates (Faucheux et al., 2004).

Insight into the cell morphology was obtained via AFM analysis. Fig. 8a - 8h displays selected AFM micrographs of the H4 for both the unmodified and SAM-modified surfaces. Fig. 8i - 8p shows representations of the AFM micrographs recorded for the PC12. Although some subtle differences in cell morphology exist, both cell lines exhibited similar trends. For the bare 6H-SiC and 1-octadecene modified surfaces, AFM micrographs showed elongated

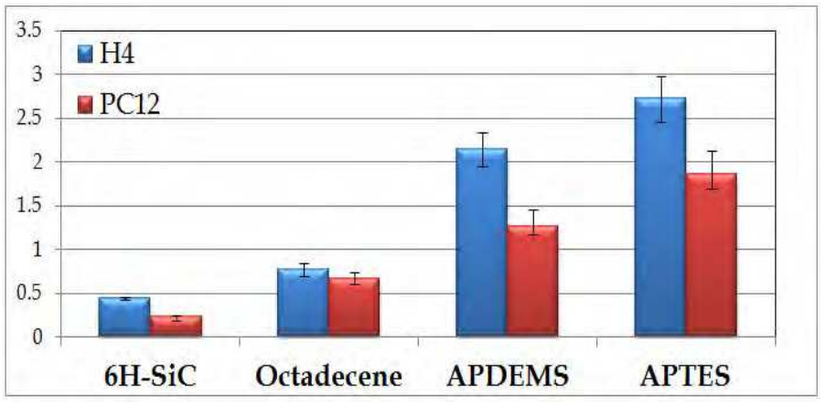

Fig. 7. Relative viability of the H4 and PC12 on the (0001) 6H-SiC as a function of surface termination as determined by MTT assay. The results are expressed as SDM ($\bar{x}$) and SEM (σ_M) and normalized to the PSt readings (Oliveros et al., 2009).

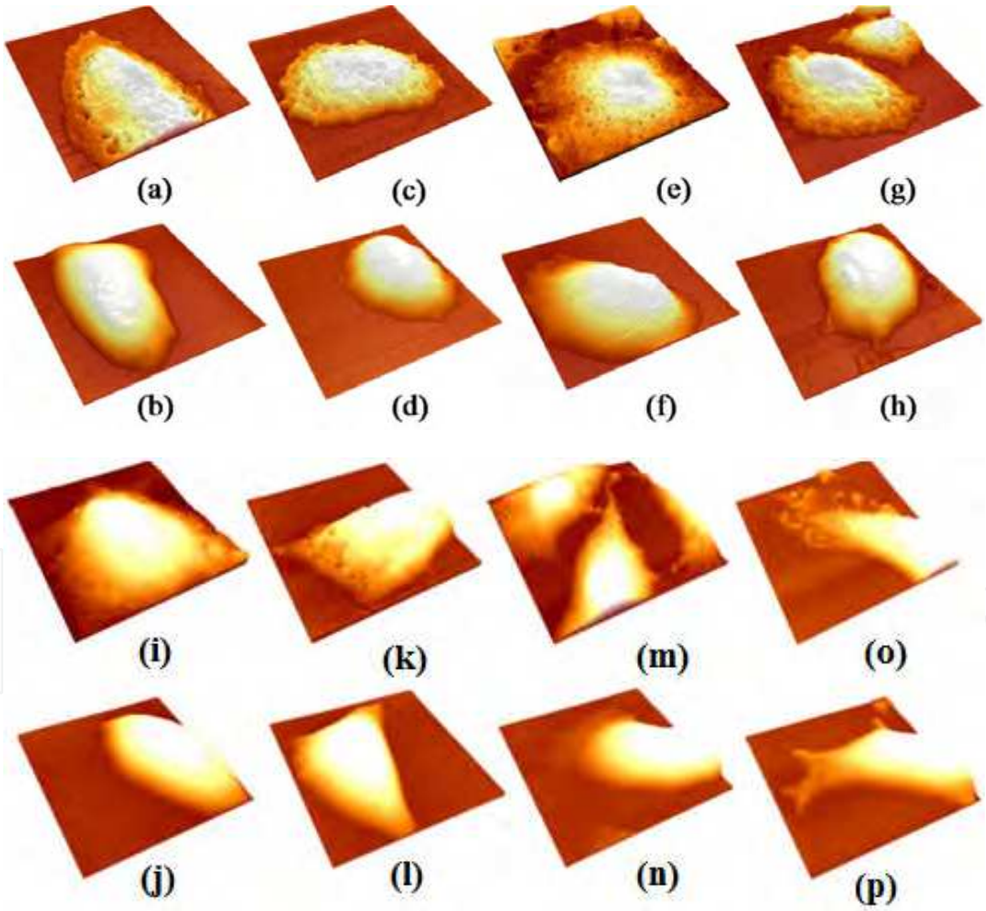

Fig. 8. 45µm x 45µm AFM micrographs for H4 (a – h) & PC12 (i – p) that are fixed (top row) and live (bottom row). (a, b, i, & j) are untreated 6H-SiC, (c, d, k, & l) are 6H-SiC after with 1-octadecene, (e, f, m, & n) are 6H-SiC with APDEMS, and (g, h, o, & p) are 6H-SiC with APTES (Oliveros et al., 2009).

or rounded cells with few focal points, filopodia, and lamellipodia extensions. Indeed, the lamellipodia areas seen on those surfaces were not significant with respect to the total cellular areas (Fig. 8). Conversely, on the APDEMS and APTES treated surfaces, we observed elongated and flattened cells that expanded over large surface areas, suggesting good attachment and consistent with the high proliferation observed using MTT assays (Fig. 7). Additionally, there was evidence of focal point attachment, filopodia and lamellipodia extensions, as well as intercellular interaction. These results compliment the MTT assays which showed greater proliferation on these surfaces compared to the untreated and 1-octadecene modified 6H-SiC surfaces.

3.3 Discussion

Cell attachment and proliferation on surfaces are the products of many chemical processes occurring between the cell membrane and the underlying substrate in contact with the cell. This involves chemical, morphological, and electrical properties of the surface, as well as cell protein-receptor binding and internal cellular reactions, all of which affect the cell-biomaterial interaction (Dan, 2003; Mrksich et al., 1996). Furthermore, ECM protein adsorption on the substrate, which can occur much more rapidly than cell adhesion, is a key step in the mechanism of cell attachment and spreading (Iwata & Arima, 2007; Ostuni et al., 1999). In general, cell attachment and proliferation are considered to occur in three stages: I) protein adsorption onto the substrate from the cell medium, II) attachment and spreading of cells on the protein-modified surface and, III) remodeling of the surface by the cells through cellular protein generation (Ostuni et al., 1999). Modification of surfaces with SAMs is thought to primarily impact the first stage, since hydrophobic, electrostatic, and chemical interactions between molecular end-groups and proteins in the growth medium significantly alter the orientation, composition, and amount of attached proteins, along with the strength of adhesion (Iwata & Arima, 2007; Ostuni et al., 1999).

Here, we have modified (0001) 6H-SiC surfaces, which are hydrophilic in their untreated state (~19° SWCA), with 1-octadecene, which possesses hydrophobic methyl endgroups (~100° SWCA), and APDEMS and APTES, which possess mildly hydrophilic amine endgroups (~50° SWCA). Cell proliferation was significantly higher on the amine terminated SAMs compared to the methyl terminated SAMs and untreated. These findings are in accordance with results obtained on amino terminated SAMs on other substrates by (Faucheux et al., 2004; Lee, M.H. et al., 2005; Low et al., 2006).

Morphological evaluation of cells provides another criterion to determine permissiveness, cellular attachment, and spreading. Elongated and flat cells that are spread out on the surface give an indication of positive cell-surface interactions (Tresco et al., 1998). On the other hand, large cell height to area ratios (corresponding to cell somata which are far from the substrate), cell clumps, cells of round shape with small interfacial areas, and/or few lamellipodia extensions, are all symptomatic of low substrate permissiveness (Coletti et al., 2007; Frewin et al., 2009b).

In this work, the cell morphology evaluation on untreated 6H-SiC and 1-octadecene modified 6H-SiC showed, in general, rounded cell shape and a few elongated flat cells. Additionally, few lamellipodia and filopodia extensions were observed, with evidence on the 1-octadecene treated surface that cell bodies avoid contact with the surface. This is an indication that, although the cells might attach to the substrate following gravitational

settling from the medium, they do not find the appropriate conditions to spread and proliferate on the surface. In previous studies using other cell lines on alkylsilane-modified Si surfaces, similar cell morphologies were observed (Faucheux et al., 2004; Lee, M.H. et al., 2005; McClary et al., 2000).

AFM measurements of cells on both APDEMS and APTES treated surfaces showed significantly more elongation and spreading than on the untreated and 1-octadecene treated surfaces. The spreading and elongation were significantly more pronounced on the APTES functionalized surfaces. Indeed, the cells on the APTES surface exhibited a variety of shapes which were predominantly elongated. Such cell morphologies indicate spreading, short cell body-surface separations, and high adhesion to the surface similar to those reported by (Frewin et al., 2009b) for cells seeded on PSt and 3C-SiC. Additionally, we saw indications of microtubule and actin filament extensions on most of the cells seeded on the APDEMS and APTES treated substrates. These findings are similar to the cell morphology and cell spreading reported for rat hippocampal neurons (Stenger et al., 1993), PC12, epithelial (Low et al., 2006), and human fibroblast cells (Faucheux et al., 2004) on different amino-terminated surfaces. An additional study, which utilized fluorescence interference contrast microscopy, also demonstrated short cell-surface distances (~ 40 nm) of neurons of the dorsal root ganglia from rats on APTES-treated surfaces (Tiefenauer et al., 2001).

It has previously been demonstrated that very little protein adsorption, and essentially no fibronectin or vitronectin adsorption, occurs on non-ionic hydrophilic surfaces, such as the untreated 6H-SiC studied here (Faucheux et al., 2004). Conversely, significant protein adsorption, including fibronectin and vitronectin adsorption, occurs on both moderately hydrophobic (e.g. NH_2-terminal) and highly hydrophobic (e.g. CH_3-terminal) surfaces. However, for the case of hydrophobic surfaces, fibronectin receptor function is impaired due to poor fibronectin cell-binding domain accessibility (Faucheux et al., 2004; McClary et al., 2000). Furthermore, competitive adsorption of non-binding proteins, such as serum albumin, reduces the coverage of the ECM proteins which are important for cell spreading and proliferation on hydrophobic surfaces (McClary et al., 2000; Tresco et al., 1998). Thus, in terms of wettability, moderately hydrophilic surfaces provide a balance which allows significant ECM protein adsorption while retaining appropriate integrin function.

In addition to protein adsorption, direct cell-surface interactions should also be considered. It has been previously reported that cells show a tendency to attach to positively charged surfaces (Dan, 2003; Van Damme et al., 1994) and that surface charge may modulate cell attachment and spreading, as found by (Tresco et al., 1998) in their study of thiols, amines, and quaternary amines. In principle, such an effect could contribute to the differences in cell proliferation observed on untreated, CH_3 and NH_2 terminal surfaces (Tresco et al., 1998). In order to affirm that the behavior of the cells presented above is general to other cell types, and to ascertain the roles of electrostatic forces and surface chemistry, additional studies on surface-modified SiC will be required.

3.4 Conclusion

Although SiC has already seen some implementation in modern medical implants (Li et al., 2005), and previous studies have suggested that SiC is biocompatible with different cell lines (Coletti et al., 2007; Frewin et al., 2009b; Li et al., 2005), little research has been devoted to

enhancing its biocompatibility via surface modification. In this work, we examined the possibility of increasing cellular proliferation and attachment on the (0001) Si face of 6H-SiC with PC12 and H4 using SAM with terminal methyl and amino groups. Our observations confirmed the influence of the substrate on viability and permissiveness, which were significantly better for the amino terminated surfaces compared to the alkyl terminated surfaces. Indeed, significant increases of cell proliferation were obtained using mildly hydrophilic amino-terminal monolayers; the APTES (APDEMS) modified surfaces exhibited an increase by a factor of ~5x (~3x) for the PC12 and ~8x (~6x) for the H4 with respect to untreated 6H-SiC. Only a moderate increase of the cell viability was observed on hydrophobic 1-octadecene modified surfaces.

This study indicates that the application of SAMs on 6H-SiC can greatly increase cell viability and substrate permissiveness while providing the ability to modify specific surface properties (Stutzmann et al., 2006). This method allows for direct control of the wettability along with surface reactivity and charge which can directly mediate cell adhesion and spreading.

4. Cellular interactions on graphene

Carbon allotropes, specifically carbon nanotubes (CNTs) and graphene have proven to be promising candidates for biological implants as they potentially combine good biocompatibility with excellent chemical resistance (Chen et al., 2008). Even though CNTs have been studied and applied in tissue engineering and biosensing (Yang et al., 2010), there are still some concerns regarding their biocompatibility (Pumera, 2009). On the other hand, although graphene is considered to be a relatively new material, it is well known for its exceptional electrical, thermal and mechanical properties (Geim & Novoselov, 2007), as well as for its high sensitivity to chemical environments (Novoselov et al., 2007). While graphene is an appealing candidate for biomedical applications its biocompatibility must first be assessed and established.

There are different ways to prepare graphene, such as mechanical cleaving, chemical synthesis, epitaxial growth on SiC, and CVD (chemical vapor deposition) on metals. Each process yields graphene with different electrical, optical and morphological properties. In Factors such as the interaction with the substrate, the presence of impurities, and the physical edge of the structure, as well as ultimately the number of layers formed, define the final properties of graphene (Geim & Novoselov, 2007). The epitaxial growth of graphene on SiC in an Ar environment produces high quality films with large domains and good thickness control, with the additional advantage of not having to physically transfer the graphene film to an insulating substrate (Emtsev et al., 2009).

To date, only a few reports discuss the biocompatibility of chemically prepared graphene derivatives (Agarwal et al., 2010; Chen et al., 2008). Recently a study of the biocompatibility of single layer graphene produced by CVD on Cu using human osteoblasts and mesenchymal stromal cells has reported better cell proliferation and morphology compared as to SiO_2/Si surfaces (Kalbac et al., 2010). 6H-SiC has been shown to be biocompatible (Coletti et al., 2007) but it has not been reported if the graphitization of this surface will present a similar behavior. This subsection presents our initial assessment of the biocompatibility of epitaxial graphene on (0001) 6H-SiC (Oliveros et al., 2011).

4.1 Methods and materials

The graphene films were epitaxially grown on (0001) 6H-SiC substrates. Initially, the 6H-SiC samples were H_2 etched in order to obtain a well ordered surface (Frewin et al., 2009a). Subsequently, graphitization was performed under an Ar environment at annealing temperature between 1600 and 1700 °C (Emtsev et al., 2009). The quality and thickness of the graphene films were evaluated by angle-resolved photoemission spectroscopy (ARPES) and X-ray photoelectron spectroscopy (XPS) as in (Coletti et al., 2010; Riedl et al., 2009). AFM and SWCA were used to assess the surface morphology and wettability of SiC and graphene. The SWCA was performed using the methods outlined in 3.1.

Prior to cell seeding the graphene surfaces were cleaned of possible air contamination by performing thermal annealing under an Ar atmosphere at 700°C in a chemical vapor deposition (CVD) reactor. For one set of samples (A) cell seeding was performed without any further surface treatment. Another set of samples (B) had an additional disinfection step via immersion in ethanol. The different surface treatment methods were considered with the intention of learning if the ethanol dip would change the cell morphology and proliferation. The 6H-SiC surfaces were HF dipped to remove the native oxide, annealed under the same conditions as graphene, and finally ethanol dipped.

For the cell morphology analysis and viability assays, human keratinocyte cells (HaCaT) were counted and plated at a density of $3.0x10^4$ cells/cm^2 in DMEM supplemented with 10% FBS and incubated for 72 hours. A 5 μM solution of CMFDA (5-chloromethylfluorescein-diacetate) cell tracker dye was used to examine cell morphology analysis via fluorescent microscopy (Coletti et al., 2007), and AFM measurements (1.3.2) were performed on fixed cells to evaluate the filopodia and lamellipodia extensions. Viability evaluation was performed using MTT assays (1.3.1). Immunoflourescence was performed at 48 hours (1.3.3) to investigate focal attachment and the actin cytoskeleton of the HaCaT.

4.2 Results

Characterization of the epitaxial graphene and 6H-SiC surfaces was performed to assess the surface properties prior to cell seeding. In Fig. 9a we report the dispersion of the π-bands around the K-point of the graphene Brillouin zone measured via ARPES for a typical sample used in this work. The π-bands linear dispersion and the displacement of the Fermi level above the Dirac point of circa 0.42 eV are characteristic features of monolayer graphene epitaxially grown on (0001) SiC. Also the C1s XPS spectrum reported in Fig. 9b confirms the monolayer nature of the adopted graphene films. The analysis of the graphene surface topography with AFM (see Fig. 9c) showed indication of large continuous terraces, on average 3.6 ± 2 μm long with a step height of 6.3 ± 3.6 nm, which is larger than the original H_2 etched 6H-SiC substrate terraces (data not shown) consistent with (Emtsev et al., 2009).

The SWCA measured for graphene cleaned by methods A and B were 87.3° ± 9.5° and 94.9° ± 3.2°, respectively. These results confirm the hydrophobicity of graphene (Wang et al., 2009) and demonstrate that ethanol disinfection did not change the water affinity of the surface significantly. For 6H-SiC the SWCA was 47°.2 ± 3°, confirming the hydrophilic character of the surface in support of previous reported data (Coletti et al., 2007).

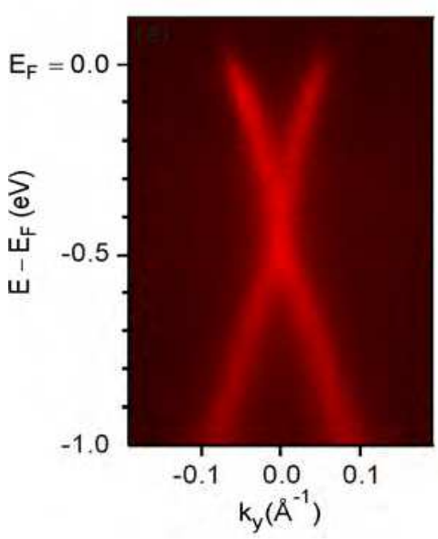

(a)

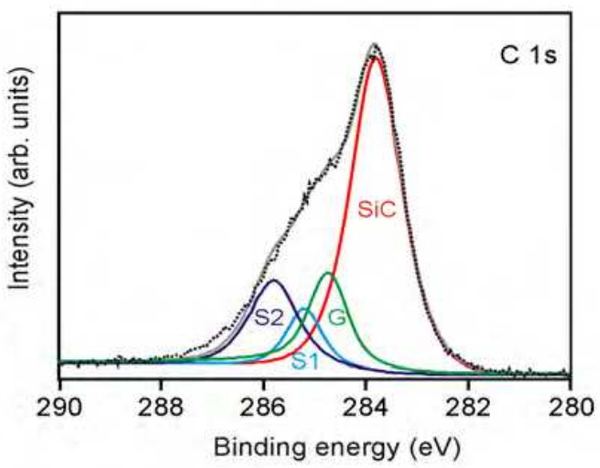

(b)

(c)

Fig. 9. ARPES (a) and XPS (b) characterization of a monolayer graphene sample. (a) Dispersion of the π-bands measured with UV excited ARPES (hν = 40.8 eV) with a display analyzer oriented for momentum scans perpendicular to the ΓK-direction of the graphene Brillouin zone. (b) C1s XPS spectrum measured using a non-monochromatic Mg Kα source, hν = 1253.6 eV, plotted as a black line and fitted components. (c) 20 µm x 20 µm AFM micrograph of epitaxial graphene on 6H-SiC (0001). Z scale -10 nm to 8 nm (Oliveros et al., 2011).

After 72 hours, for both graphene and 6H-SiC, the morphology of the HaCaT cells was similar to that on the PSt control (data not shown) with signs of cell-cell interaction and cell-substrate interaction (Fig. 10). The cells appeared to be flattened and cuboidal typical of HaCaT cells. The morphology is confirmed with AFM inspection shown in Fig. 11a & 11b where the filopodia and lamellipodia of the cells have been identified. In addition, immunofluorescence analysis of the actin cytoskeleton and the number of focal points are shown in Fig. 11c. These indicate some HaCaT cells present elongated shape while others are a more cubical. We can see the actin fibers (red) are oriented towards the focal points localization (green), indicating good surface attachment.

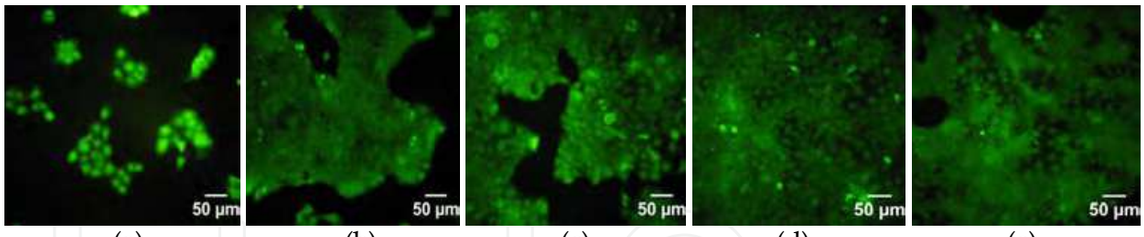

(a) (b) (c) (d) (e)

Fig. 10. Fluorescent micrographs of HaCaTs after 72 hour on a) graphene (A), b) graphene (B), c) 6H-SiC(0001), and after 120 hrs on d) 6H-SiC(0001) and e) graphene (B) (Oliveros et al., 2011).

4.3 Discussion

Certain differences were observed for cell proliferation and shape when seeded on surfaces after ethanol disinfection. For the graphene substrates from group A, as seen in Fig 10a, small islands of cells were observed compared to the monolayer that started forming on the graphene surface cleaned by method B (Fig 10b). The 6H-SiC samples also showed via optical inspection clear signs of an initial formation of a cell monolayer (see Fig 10c). It is apparent from the comparison of Figures 10a and 10b that the ethanol dip step favors a more homogeneous cell adhesion and for this reason subsequent experiments whose results are reported below were performed only on samples cleaned by using method B. It is known that HaCaTs tend to form groups of cells such as islands, and with time they start growing tighter and closer to each other and eventually form a conformal layer of cells. Consequently at a time of 120 hours optical inspection of cells plated graphene and 6H-SiC samples was performed with the intent of checking whether the cells would grow to confluence. Promisingly, as shown in Figures 10d & 10e, the 120 hrs optical inspection data showed a homogeneous monolayer of cells formed on both graphene and 6H-SiC.

On the other hand, the MTT assays provided an average value of cell viability after 72 hrs of incubation and with respect to the PSt control. The results were as follows: 17 ± 0.07 (std deviation of the mean) for graphene and 58 ± 0.05 for 6H-SiC. It should be pointed out that the lower viability values obtained for the graphene surfaces might be explained by the hydrophobic nature of the substrate. It may significantly contribute to the cell viability because the initial phase of cell attachment involves the physicochemical linkages between the cells and the surface through proteins (Akasaka et al., 2010). Despite the lower viability measured on graphene after 72 hours of incubation, the evidence of the formation of a cell monolayer on graphene substrates in a similar fashion to 6H-SiC (as in Figures 10d & 10e) after 120 hours of incubation strongly suggests the need to perform longer time MTT assays. As already discussed, because of the hydrophobic nature of the surface, the cells may adapt to it and find the right cues for increased cell proliferation over longer time spans (Akasaka et al., 2010). In addition, the cell viability on both surfaces was compared using an ANOVA test considering that the viability is sample dependent. In this case we obtained that, even though the graphene and 6H-SiC viability levels are close, the surfaces are statistically different with a p-value =0.043 (Oliveros et al., 2011).

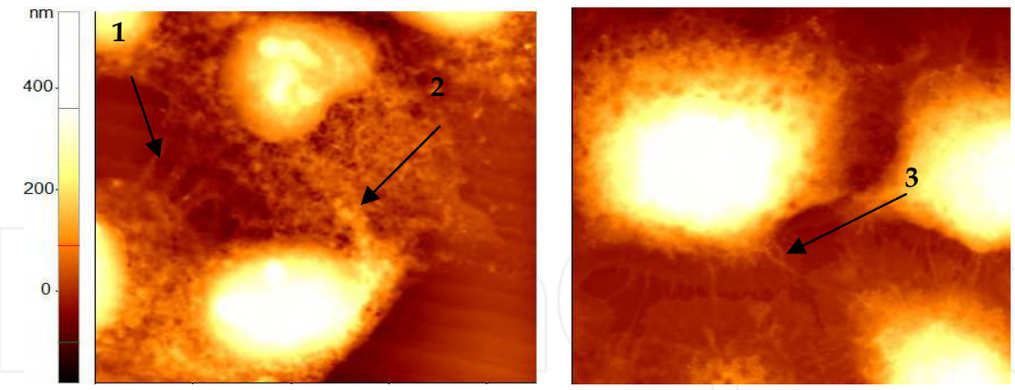

(a) (b)

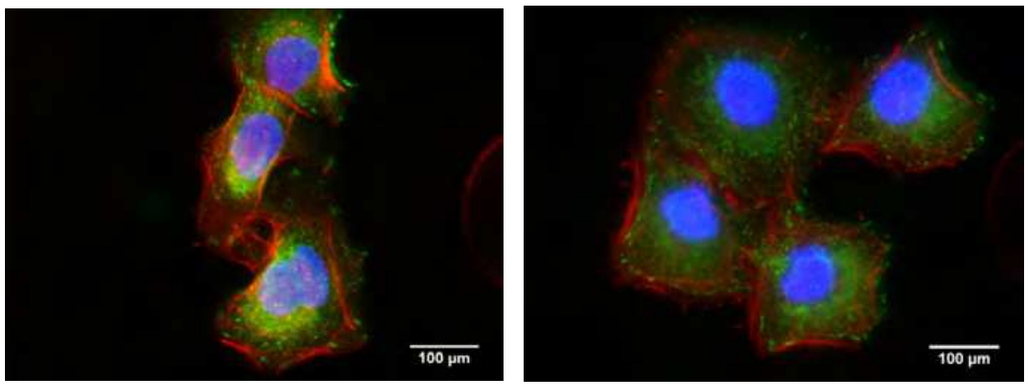

(c)

Figure 11. 45 µm x 45 µm AFM micrographs of HaCaT cells on (a) monolayer graphene and (b) H intercalated graphene. The AFM micrographs confirm the presence of 1) cell-cell interaction and 2) evidence of lamellipodia and 3) filopodia. (c) Composite images actin (red), focal points (green) and cell nuclei (blue) on epitaxial graphene (Oliveros et al., 2011).

4.4 Conclusion

In this paper we have reported preliminary methods and result for testing the in vitro biocompatibility of epitaxial graphene on (0001) 6H-SiC through the cellular interactions of HaCaT cells with these surfaces. We have compared the cell viability and cell morphology of these surfaces. Two different cleaning procedures were employed on the graphene surfaces tested. The optical inspection results after 72 hours of cell incubation suggest that the ethanol sterilization step is required in order to have a more homogeneous and enhanced cell adhesion on graphene surfaces. The results obtained from MTT assays after the same incubation time (i.e., 72 hours) evidence of cell viability almost 3 times higher for 6H-SiC than for graphene surfaces. However, the optical inspection performed after 5 days of incubation shows that cells grow in a similar trend on graphene as they do on 6H-SiC. Hence, it is possible to speculate that the viability values obtained after 3 days of incubation might be due to the initial process of surface recognition by the cell and later activation of the appropriate mechanisms for proliferation. Additional MTT assays and optical inspection over longer incubation times must be performed before giving a final answer regarding the in vitro biocompatibility level of graphene. Also, studies pertaining to the cytoskeleton

organization (e.g. actin cytoskeleton) on these surfaces or the determination of the number of contact sites (e.g. vinculin staining) could give better insight into the process of cell adhesion and proliferation on graphene.

5. Conclusion

The results of this work have shown that SiC and graphene could potentially become excellent materials for use in biomedical implants. As these materials can be opaque due to the substrates they are grown on, we have shown a method that involves AFM to study the morphology and pseudopodia extensions of cells on their surfaces. In combination with techniques that measure viability, the AFM can be an excellent tool for investigating whole cells interacting on surfaces. Combining the whole cell AFM investigation with previously developed AFM techniques of protein investigation on surfaces, one could more fully understand the cell to substrate interactions and model methods to manipulate them to improve implantable biomedical devices in the future.

6. Acknowledgment

The authors wish to thank: Florida Center of Excellence for Biomolecular Identification & Targeted Therapeutics at USF for the financial support to perform this work; S. Afroz at USF for thermal annealing; Leigh West of the USF FCoE BiTT center for his assistance with fluorescence imaging; K. Emtsev of Max Planck Institute help with the preparation of graphene samples; M. Jaroszeski of USF Engineering for cell culturing.

7. References

Agarwal, S., Zhou, X. Z., Ye, F., He, Q. Y., Chen, G. C. K., Soo, J., Boey, F., Zhang, H. & Chen, P. (2010). Interfacing Live Cells with Nanocarbon Substrates. *Langmuir*, Vol. 26, No. 4, (Feb. 16, 2010), pp. 2244-2247, ISSN 0743-7463.

Akasaka, T., Yokoyama, A., Matsuoka, M., Hashimoto, T. & Watari, F. (2010). Thin films of single-walled carbon nanotubes promote human osteoblastic cells (Saos-2) proliferation in low serum concentrations. *Materials Science and Engineering C*, Vol. 30, No. 3, pp. 391-399, ISSN 0928-4931.

Bergkvist, M., Carlsson, J. & Oscarsson, S. (2003). Surface-dependent conformations of human plasma fibronectin adsorbed to silica, mica, and hydrophobic surfaces, studied with use of Atomic Force Microscopy. *Journal of Biomedical Materials Research Part A*, Vol. 64A, No. 2, (Feb 1, 2003), pp. 349-356, ISSN 0021-9304.

Birchall, J. D. & Chappell, J. S. (1988). The Chemistry of Aluminum and Silicon in Relation to Alzheimers-Disease. *Clinical Chemistry*, Vol. 34, No. 2, (Feb., 1988), pp. 265-267, ISSN 0009-9147.

Booth, M. J., Ju, R. & Wilson, T. (2008). Spectral confocal reflection microscopy using a white light source. *Journal of the European Optical Society*, Vol. 3, No. 1, (Aug. 20, 2008), pp. 08026-1-6, ISSN 1990-2573.

Boppart, S. A., Wheeler, B. C. & Wallace, C. S. (1992). A Flexible Perforated Microelectrode Array for Extended Neural Recordings. *IEEE Transactions on Biomedical Engineering*, Vol. 39, No. 1, (Jan., 1992), pp. 37-42, ISSN 0018-9294.

Carlisle, E. M. (1986). Silicon as an Essential Trace-Element in Animal Nutrition, In: *Ciba Foundation Symposia 121 - Silicon Biochemistry*, Evered, D. & O'connor, M. (eds.), pp. 123-139, John Wiley & Sons, Ltd., ISBN 0300-5208, Chichester, UK.

Catellani, A. & Cicero, G. (2007). Modifications of cubic SiC surfaces studied by ab initio simulations: from gas adsorption to organic functionalization. *Journal of Physics D - Applied Physics*, Vol. 40, No. 20, (Oct 21, 2007), pp. 6215-6224, ISSN 0022-3727.

Chen, H., Muller, M. B., Gilmore, K. J., Wallace, G. G. & Li, D. (2008). Mechanically strong, electrically conductive, and biocompatible graphene paper. *Advanced Materials*, Vol. 20, No. 18, (Sep. 17, 2008), pp. 3557-3561, ISSN 0935-9648.

Clark, P., Britland, S. & Connolly, P. (1993). Growth Cone Guidance and Neuron Morphology on Micropatterned Laminin Surfaces. *Journal of Cell Science*, Vol. 105, No. 1, (May 1, 1993), pp. 203-212, ISSN 0021-9533.

Coletti, C., Jaroszeski, M. J., Pallaoro, A., Hoff, A. M., Iannotta, S. & Saddow, S. E. (2007). Biocompatibility and wettability of crystalline SiC and Si surfaces, *Proceedings of IEEE Engineering in Medicine and Biology Society*, ISBN 1557-170X, Lyon, FR, 22 - 26 Aug., 2007

Coletti, C., Riedl, C., Lee, D. S., Krauss, B., Patthey, L., Von Klitzing, K., Smet, J. H. & Starke, U. (2010). Charge neutrality and band-gap tuning of epitaxial graphene on SiC by molecular doping. *Physical Review B*, Vol. 81, No., pp. 235401-1- 235401-8.

Dan, N. (2003). The effect of charge regulation on cell adhesion to substrates: salt-induced repulsion. *Colloids and Surfaces B-Biointerfaces*, Vol. 27, No. 1, (Jan., 2003), pp. 41-47, ISSN 0927-7765.

Donoghue, J. P. (2008). Bridging the brain to the world: a perspective on neural interface systems. *Neuron*, Vol. 60, No. 3, (Nov. 6, 2008), pp. 511-521, ISSN 1097-4199 (Electronic); 0896-6273 (Linking).

Easley Iv, C. A., Brown, C. M., Horwitz, A. F. & Tombes, R. M. (2008). CaMK-II promotes focal adhesion turnover and cell motility by inducing tyrosine dephosphorylation of FAK and paxillin. *Cell Motility and the Cytoskeleton*, Vol. 65, No. 8, (Aug., 2008), pp. 662-674, ISSN 0886-1544.

Emtsev, K. V., Bostwick, A., Horn, K., Jobst, J., Kellogg, G. L., Ley, L., Mcchesney, J. L., Ohta, T., Reshanov, S. A., Rohrl, J., Rotenberg, E., Schmid, A. K., Waldmann, D., Weber, H. B. & Seyller, T. (2009). Towards wafer-size graphene layers by atmospheric pressure graphitization of silicon carbide. *Nature Materials*, Vol. 8, No. 3, (Mar., 2009), pp. 203-207, ISSN 1476-1122.

Faucheux, N., Schweiss, R., Lutzow, K., Werner, C. & Groth, T. (2004). Self-assembled monolayers with different terminating groups as model substrates for cell adhesion studies. *Biomaterials*, Vol. 25, No. 14, (Jun., 2004), pp. 2721-2730, ISSN 0142-9612.

Fawcett, J. W. & Asher, R. A. (1999). The glial scar and central nervous system repair. *Brain Research Bulletin*, Vol. 49, No. 6, (May 14, 1999), pp. 377-391, ISSN 0361-9230.

Fine, E. G., Valentini, R. F., Bellamkonda, R. & Aebischer, P. (1991). Improved Nerve Regeneration through Piezoelectric Vinylidenefluoride-Trifluoroethylene Copolymer Guidance Channels. *Biomaterials*, Vol. 12, No. 8, (Oct., 1991), pp. 775-780, ISSN 0142-9612.

Frame, M. C., Fincham, V. J., Carragher, N. O. & Wyke, J. A. (2002). v-Src's hold over actin and cell adhesions. *Nature Reviews Molecular Cell Biology*, Vol. 3, No. 4, (Apr., 2002), pp. 233-245, ISSN 1471-0072.

Frewin, C. L., Coletti, C., Riedl, C., Starke, U. & Saddow, S. E. (2009a). A Comprehensive Study of Hydrogen Etching on the Major SiC Polytypes and Crystal Orientations. *Materials Science Forum*, Vol. 615-617, No. -, (Mar., 2009), pp. 589 - 592.

Frewin, C. L., Jaroszeski, M., Weeber, E., Muffly, K. E., Kumar, A., Peters, M., Oliveros, A. & Saddow, S. E. (2009b). Atomic force microscopy analysis of central nervous system cell morphology on silicon carbide and diamond substrates. *Journal of Molecular Recognition*, Vol. 22, No. 5, (Sep-Oct., 2009), pp. 380-388, ISSN 0952-3499.

Geim, A. K. & Novoselov, K. S. (2007). The rise of graphene. *Nature Materials*, Vol. 6, No. 3, (Mar., 2007), pp. 183-191, ISSN 1476-1122.

Gordon-Weeks, P. R. (2004). Microtubules and growth cone function. *Journal of Neurobiology*, Vol. 58, No. 1, (Jan., 2004), pp. 70-83, ISSN 0022-3034.

Hench, L. L. & Wilson, J. (1986). Biocompatibility of silicates for medical use, In: *Ciba Foundation Symposium 121 - Silicon Biochemistry*, Evered, D. & O'connor, M. (eds.), pp. 231–253, John Wiley & Sons, ISBN 0300-5208 Chichester, UK.

ISO-10993-1 (2009), Biological evaluation of medical devices Part 1: Evaluation and testing, International Standards Orginization, Geneva, Switzerland.

ISO-10993-5 (2009), Biological evaluation of medical devices Part 5: Tests for in vitro cytotoxicity, International Standards Orginization, Geniva, Switzerland.

ISO-10993-6 (2007), Biological evaluation of medical devices Part 6: Tests for local effects after implantation, International Standards Orginization, Geneva, Switzerland.

Iwata, H. & Arima, Y. (2007). Effects of surface functional groups on protein adsorption and subsequent cell adhesion using self-assembled monolayers. *Journal of Materials Chemistry*, Vol. 17, No. 38, pp. 4079-4087, ISSN 0959-9428.

Juliano, R. L. & Haskill, S. (1993). Signal transduction from the extra cellular matrix. *Journal of Cell Biology*, Vol. 120, No. 3, (Feb. 1,), pp. 577-585, ISSN 0021-9525.

Kalbac, M., Kalbacova, M., Broz, A. & Kong, J. (2010). Graphene substrates promote adherence of human osteoblasts and mesenchymal stromal cells. *Carbon*, Vol. 48, No. 15, (Dec., 2010), pp. 4323-4329, ISSN 0008-6223.

Kalnins, U., Erglis, A., Dinne, I., Kumsars, I. & Jegere, S. (2002). Clinical outcomes of silicon carbide coated stents in patients with coronary artery disease. *Medical Science Monitor*, Vol. 8, No. 2, (Feb. 23, 2002), pp. PI16-20, ISSN 1234-1010.

Kapur, R. & Rudolph, A. S. (1998). Cellular and cytoskeleton morphology and strength of adhesion of cells on self-assembled monolayers of organosilanes. *Experimental Cell Research*, Vol. 244, No. 1, (Oct. 10, 1998), pp. 275-285, ISSN 0014-4827.

Kim, K. H., Cho, J. S., Choi, D. J. & Koh, S. K. (2001). Hydrophilic group formation and cell culturing on polystyrene Petri-dish modified by ion-assisted reaction. *Nuclear Instruments & Methods in Physics Research Section B*, Vol. 175-177, No. -, (Apr., 2001), pp. 542-547, ISSN 0168-583X.

Kordina, O. & Saddow, S. E. (2004). Silicon carbide overview, In: *Advances in Silicon Carbide Processing and Applications*, Saddow, S. E. & Agarwal, A. (eds.), pp. 2–3,7–8,18, Artech House, Inc., ISBN 1580537405, Boston, MA, U.S.A.

Kumar, A., Ahmed, I. & Vedawyas, M. (2000). Growth of diamond films on Ti-6Al-4V substrates and determination of residual stresses using Raman spectroscopy. *Journal of Vacuum Science & Technology a-Vacuum Surfaces and Films*, Vol. 18, No. 5, (Sep. 2000), pp. 2486 – 2492, ISSN 0734-2101.

Kumari, T. V., Vasudev, U., Kumar, A. & Menon, B. (2002). Cell surface interactions in the study of biocompatibility. *Trends in Biomaterials & Artificial Organs*, Vol. 15, No. 2, pp. 37-41.

Lee, K. K., He, J. P., Singh, A., Massia, S., Ehteshami, G., Kim, B. & Raupp, G. (2004). Polyimide-based intracortical neural implant with improved structural stiffness. *Journal of Micromechanics and Microengineering*, Vol. 14, No. 1, (Jan., 2004), pp. 32-37, ISSN 0960-1317.

Lee, M. H., Brassb, D. A., Morris, R., Composto, R. J. & Ducheyne, P. (2005). The effect of non-specific interactions on cellular adhesion using model surfaces. *Biomaterials*, Vol. 26, No. 14, (July 20, 2004), pp. 1721-1730, ISSN 0142-9612.

Levitan, I. B. & Kaczmarek, L. K. (2002). *The Neuron - Cell and Molecular Biology* (3), Oxford University Press:, ISBN 0-19-514523-2, New York, New York.

Li, X., Wang, X., Bondokov, R., Morris, J., An, Y. H. & Sudarshan, T. S. (2005). Micro/nanoscale mechanical and tribological characterization of SiC for orthopedic applications. *Journal of Biomedical Materials Research Part B: Applied Biomaterials*, Vol. 72, No. 2, (Feb. 15, 2005), pp. 353–361, ISSN 1552-4973.

Linford, M. R. & Chidsey, C. E. D. (1993). Alkyl Monolayers Covalently Bonded to Silicon Surfaces. *Journal of the American Chemical Society*, Vol. 115, No. 26, (Dec. 29, 1993), pp. 12631-12632, ISSN 0002-7863.

Locke, C., Kravchenko, G., Waters, P., Reddy, J. D., Du, K., Volinsky, A. A., Frewin, C. L. & Saddow, S. E. (2009). 3C-SiC Films on Si for MEMS Applications: Mechanical Properties. *Material Science Forum*, Vol. 615-617, No. -, pp. 633-636.

Low, S. P., Williams, K. A., Canham, L. T. & Voelcker, N. H. (2006). Evaluation of mammalian cell adhesion on surface-modified porous silicon. *Biomaterials*, Vol. 27, No. 26, (Sep., 2006), pp. 4538-4546, ISSN 0142-9612.

Makohliso, S. A., Valentini, R. F. & Aebischer, P. (1993). Magnitude and Polarity of a Fluoroethylene Propylene Electret Substrate Charge Influences Neurite Outgrowth in-Vitro. *Journal of Biomedical Materials Research*, Vol. 27, No. 8, (Aug., 1993), pp. 1075-1085, ISSN 0021-9304.

Mcclary, K. B., Ugarova, T. & Grainger, D. W. (2000). Modulating fibroblast adhesion, spreading, and proliferation using self-assembled monolayer films of alkylthiolates on gold. *Biomedical Materials Research*, Vol. 50, No. 3, (Jun. 5, 2000), pp. 428-439, ISSN 0021-9304.

Miyamoto, S., Akiyama, S. K. & Yamada, K. M. (1995). Synergistic roles form receptor occupancy and aggregation in integrin transmembrane function. *Science*, Vol. 267, No. 5199, (Feb. 10, 1995), pp. 883–885.

Mosmann, T. (1983). Rapid colorimetric assay for cellular growth and survival: application to proliferation and cytotoxicity assays. *Journal of Immunological Methods*, Vol. 65, No. 1-2, (Dec. 16, 1983), pp. 55-63, ISSN 0022-1759.

Mrksich, M., Chen, C. S., Xia, Y., Dike, L. E., Ingber, D. E. & Whitesides, G. M. (1996). Controlling cell attachment on contoured surfaces with self-assembled monolayers of alkanethiolates on gold. *Proceedings of the National Academy of Sciences of the United States of America*, Vol. 93, No. 20, (Oct. 1, 1996), pp. 10775-8, ISSN 0027-8424.

Mrksich, M. & Whitesides, G. M. (1996). Using self-assembled monolayers to understand the interactions of man-made surfaces with proteins and cells. *Annual review of*

biophysics and biomolecular structure, Vol. 25, No. -, (Jun., 1996), pp. 55-78, ISSN 1056-8700.

Novoselov, K. S., Schedin, F., Geim, A. K., Morozov, S. V., Hill, E. W., Blake, P. & Katsnelson, M. I. (2007). Detection of individual gas molecules adsorbed on graphene. *Nature Materials*, Vol. 6, No. 9, (Sep., 2007), pp. 652-655, ISSN 1476-1122.

Oliveros, A., Coletti, C., Frewin, C. L., Locke, C., Starke, U. & Saddow, S. E. (2011). Cellular Interactions on Epitaxial Graphene on SiC (0001) Substrates. *Material Science Forum*, Vol. 679-680, No. -, pp. 831-834.

Oliveros, A., Schoell, S. J., Frewin, C., Hoeb, M., Stutzmann, M., Sharp, I. D. & Saddow, S. E. (2009). Biocompatibility Assessment of SiC Surfaces After Functionalization with Self Assembled Organic Monolayers *Materials Research Society Symposium Proceedings*, Vol. 1235, No. -, pp. 1235-RR03-43-48.

Ostrovskaya, L., Perevertailo, V., Ralchenko, V., Saveliev, A. & Zhuravlev, V. (2007). Wettability of nanocrystalline diamond films. *Diamond and Related Materials*, Vol. 16, No. 12, (Dec., 2007), pp. 2109-2113, ISSN 0925-9635.

Ostuni, E., Yan, L. & Whitesides, G. M. (1999). The interaction of proteins and cells with self-assembled monolayers of alkanethiolates on gold and silver. *Colloids and Surfaces B-Biointerfaces*, Vol. 15, No. 1, (Aug. 31, 1999), pp. 3-30, ISSN 0927-7765.

Polikov, V. S., Tresco, P. A. & Reichert, W. M. (2005). Response of brain tissue to chronically implanted neural electrodes. *Journal of Neuroscience Methods*, Vol. 148, No. 1, (Aug. 8, 2005), pp. 1-18, ISSN 0165-0270.

Pumera, M. (2009). Electrochemistry of Graphene: New Horizons for Sensing and Energy Storage. *Chemical Record*, Vol. 9, No. 4, (Sep. 8, 2009), pp. 211-223, ISSN 1527-8999.

Reyes, M., Shishkin, Y., Harvey, S. & Saddow, S. E. (2006). Development of a high-growth rate 3C-SiC on Si CVD process. *Materials Research Society Symposium Proceedings*, Vol. 911, No. -, pp. 79–84.

Richards, R. G. (1996). The effect of surface roughness on fibroblast adhesion in vitro. *Injury*, Vol. 27 Suppl 3, No., (Jan. 1, 1996), pp. SC38-43, ISSN 0020-1383.

Riedl, C., Coletti, C., Iwasaki, T., Zakharov, A. A. & Starke, U. (2009). Quasi-Free-Standing Epitaxial Graphene on SiC Obtained by Hydrogen Intercalation. *Physical Review Letters*, Vol. 103, No. 24, (Dec. 11, 2009), pp. 1-4, ISSN 0031-9007.

Rosenbloom, A. J., Sipe, D. M., Shishkin, Y., Ke, Y., Devaty R. P. & Choyke, W. J. (2004). Nanoporus SiC: A Candidate Semi-Permeable Material for Biomedical Applications. *Biomedical Microdevices*, Vol. 6, No. 4, (Dec., 2004), pp. 261-267, ISSN 1387-2176.

Rouhi, A. M. (1999). Contemporary biomaterials. *Chemical & Engineering News*, Vol. 77, No. 3, (Jan. 18, 1999), pp. 51–63, ISSN 0009-2347.

Rousche, P. J. & Normann, R. A. (1998). Chronic recording capability of the Utah Intracortical Electrode Array in cat sensory cortex. *Journal of Neuroscience Methods*, Vol. 82, No. 1, (Jul. 1,1998), pp. 1-15, ISSN 0165-0270.

Rousche, P. J., Pellinen, D. S., Pivin, D. P., Williams, J. C., Vetter, R. J. & Kipke, D. R. (2001). Flexible polyimide-based intracortical electrode arrays with bioactive capability. *IEEE Transactions on Biomedical Engineering*, Vol. 48, No. 3, (Mar., 2001), pp. 361-371, ISSN 0018-9294.

Schoell, S. J., Hoeb, M., Sharp, I. D., Steins, W., Eickhoff, M., Stutzmann, M. & Brandt, M. S. (2008). Functionalization of 6H-SiC surfaces with organosilanes. *Applied Physics Letters*, Vol. 92, No. 15, (Apr. 14, 2008), pp. 92-94, ISSN 0003-6951.

Sharp, I. D., Schoell, S. J., Hoeb, M., Brandt, M. S. & Stutzmann, M. (2008). Electronic properties of self-assembled alkyl monolayers on Ge surfaces. *Applied Physics Letters*, Vol. 92, No. 92-94, (Jun 2, 2008), pp. -, ISSN 0003-6951.

Sklodowaka, A., Wozniak, M. & Matlakowska, R. (1999). The method of contact angle measurements and estimation of work of adhesion in bioleaching of metals. *Biological Procedures Online*, Vol. 1, No. -, (Apr. 29, 1999), pp. 114-121, ISSN 1480-9222.

Stenger, D. A., Pike, C. J., Hickman, J. J. & Cotman, C. W. (1993). Surface determinants of neuronal survival and growth on self-assembled monolayers in culture. *Brain Research*, Vol. 630, No. 1-2, (Dec. 10, 1993), pp. 136-47, ISSN 0006-8993.

Stichel, C. C. & Müller, H. W. (1998). The CNS lesion scar: new vistas on an old regeneration barrier. *Cell and Tissue Research*, Vol. 294, No. 1, (Oct., 1998), pp. 1-9, ISSN 0302-766X.

Stutzmann, M., Garrido, J. A., Eickhoff, M. & Brandt, M. S. (2006). Direct biofunctionalization of semiconductors: A survey. *Physica Status Solidi a-Applications and Materials Science*, Vol. 203, No. 14, (Nov., 2006), pp. 3424-3437, ISSN 0031-8965.

Tiefenauer, L., Sorribas, H., Braun, D., Leder, L. & Sonderegger, P. (2001). Adhesion proteins for a tight neuron-electrode contact. *Journal of Neuroscience Methods*, Vol. 104, No. 2, (Jan. 15, 2001), pp. 133-141, ISSN 0165-0270.

Tresco, P. A., Webb, K. & Hlady, V. (1998). Relative importance of surface wettability and charged functional groups on NIH 3T3 fibroblast attachment, spreading, and cytoskeletal organization. *Journal of Biomedical Materials Research*, Vol. 41, No. 3, (Sep. 5, 1998), pp. 422-430, ISSN 0021-9304.

Underwood, P. A., Steele, J. G. & Dalton, B. A. (1993). Effects of polystyrene surface chemistry on the biological activity of solid phase fibronectin and vitronectin, analyzed with monoclonal antibodies. *Journal of Cell Science*, Vol. 104, No. -, (Mar. 1, 1993), pp. 793-803, ISSN 0021-9533.

Vahlberg, C., Yazdi, G. R., Petoral Jr., R. M., Syväjärvi, M., Uvdal, K., Lloyd-Spetz, A., Yakimova, R. & Khranovsky, V. (2005). Surface engineering of functional materials for Biosensors, *Proceedings of IEEE Sensors*, ISBN 0-7803-9056-3, Irvine, CA, USA, Oct. 30-Nov. 3, 2005.

Van Damme, M., Tiglias, J., Nemat, N. & Preston, B. (1994). Determination of cell charge content at the surface of cells using a colloid titration technique. *Analytical Biochemistry*, Vol. 223, No. 1, (Nov. 15,1994), pp. 62-70, ISSN 0003-2697.

Wang, S., Zhang, Y., Abidi, N. & Cabrales, L. (2009). Wettability and surface free energy of graphene films. *Langmuir*, Vol. 25, No. 18, (Sep. 15, 2009), pp. 11078-11081, ISSN 0743-7463.

Williams, D. F. (2008). On the mechanisms of biocompatibility. *Biomaterials*, Vol. 29, No. 20, (Jul., 2008), pp. 2941-2953, ISSN 0142-9612.

Williams, J. C., Rennaker, R. L. & Kipke, D. R. (1999). Long-term neural recording characteristics of wire microelectrode arrays implanted in cerebral cortex. *Brain Research Protocols*, Vol. 4, No. 3, (Dec., 1999), pp. 303-313, ISSN 1385-299X.

Yakimova, R., Petoral, R. M., Yazdi, G. R., Vahlberg, C., Spetz, A. L. & Uvdal, K. (2007). Surface functionalization and biomedical applications based on SiC. *Journal of Physics D-Applied Physics*, Vol. 40, No. 20, (Oct. 21, 2007), pp. 6435-6442, ISSN 0022-3727.

Yang, W. R., Ratinac, K. R., Ringer, S. P., Thordarson, P., Gooding, J. J. & Braet, F. (2010). Carbon Nanomaterials in Biosensors: Should You Use Nanotubes or Graphene? *Angewandte Chemie-International Edition*, Vol. 49, No. 12, (Feb. 24, 2010), pp. 2114-2138, ISSN 1433-7851.

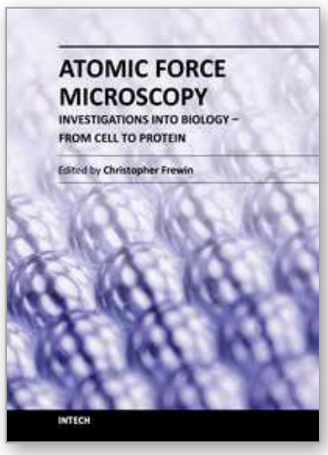

Atomic Force Microscopy Investigations into Biology - From Cell to Protein

Edited by Dr. Christopher Frewin

ISBN 978-953-51-0114-7
Hard cover, 354 pages
Publisher InTech
Published online 07, March, 2012
Published in print edition March, 2012

The atomic force microscope (AFM) has become one of the leading nanoscale measurement techniques for materials science since its creation in the 1980's, but has been gaining popularity in a seemingly unrelated field of science: biology. The AFM naturally lends itself to investigating the topological surfaces of biological objects, from whole cells to protein particulates, and can also be used to determine physical properties such as Young's modulus, stiffness, molecular bond strength, surface friction, and many more. One of the most important reasons for the rise of biological AFM is that you can measure materials within a physiologically relevant environment (i.e. liquids). This book is a collection of works beginning with an introduction to the AFM along with techniques and methods of sample preparation. Then the book displays current research covering subjects ranging from nano-particulates, proteins, DNA, viruses, cellular structures, and the characterization of living cells.

INTECH
open science | open minds

InTech Europe
University Campus STeP Ri
Slavka Krautzeka 83/A
51000 Rijeka, Croatia
Phone: +385 (51) 770 447
Fax: +385 (51) 686 166
www.intechopen.com

InTech China
Unit 405, Office Block, Hotel Equatorial Shanghai
No.65, Yan An Road (West), Shanghai, 200040, China
中国上海市延安西路65号上海国际贵都大饭店办公楼405单元
Phone: +86-21-62489820
Fax: +86-21-62489821

IntechOpen